Supplementary figures

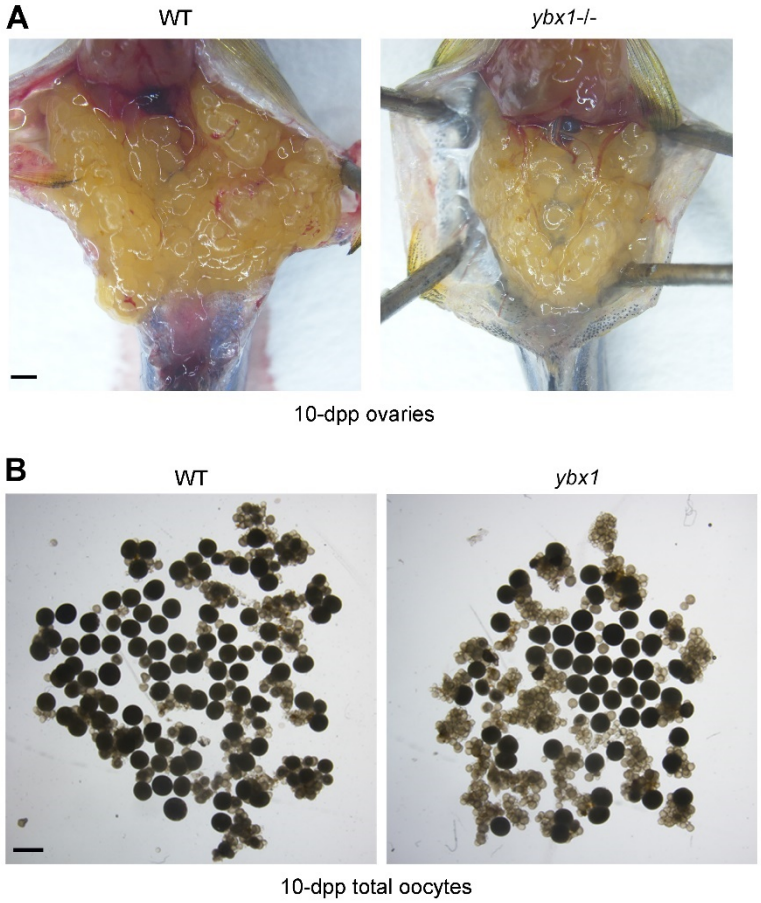

Fig. S1. Ovaries and oocytes from WT and *Zybx1* females. (A) Ovaries from WT and *Zybx1* females at 10 dpp. Mature eggs were purged from female fish via natural matings on Day 1. On Day 11 (10 dpp), female fish were sacrificed. (B) Total oocytes from WT and *Zybx1* female fish at 10 dpp. Scale bars: 1 mm.

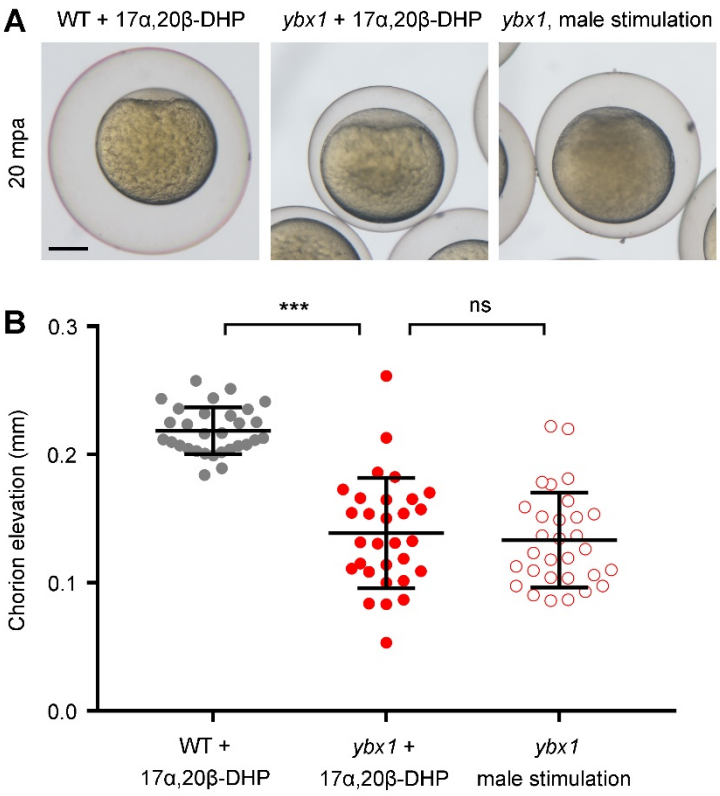

Fig. S2. Hormonal stimulation cannot rescue the egg activation defect caused by Ybx1 depletion. (A) Representative images of activated eggs with chorions. Eggs from 17α,20β-DHP-treated WT female fish, 17α,20β-DHP-treated Z*ybx1* female fish and male fish-stimulated Z*ybx1* female fish are shown from left to right. mpa, minutes post-activation. Chorion expansion after water activation was used as the criterion for evaluating oocyte maturation and egg activation. (B) Measurement of chorion elevation distances at 20 mpa. ns, not significant; ***P<0.001; Welch's t-test.

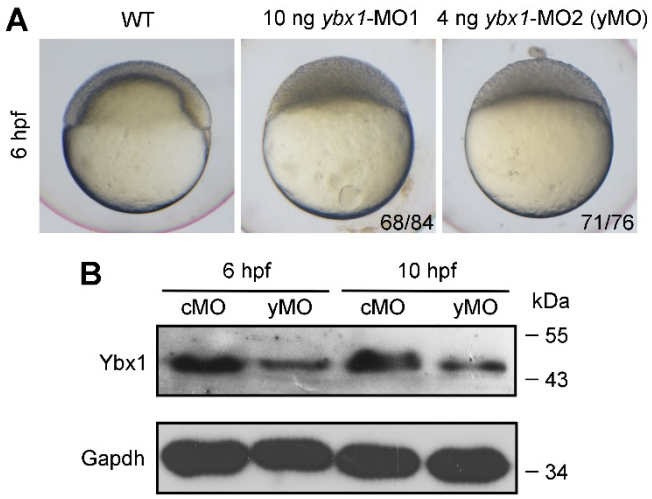

Fig. S3. Knockdown of *ybx1* expression by translation-blocking morpholinos. (A) Bright-field images of a WT embryo and embryos injected with 10 ng *ybx1*-MO1 or 4 ng *ybx1*-MO2. 4 ng *ybx1*-MO2 was injected in subsequently described experiments as yMO. (B) Examination of yMO-mediated *ybx1* knockdown efficiency. Endogenous Ybx1 and Gapdh were detected by western blotting.

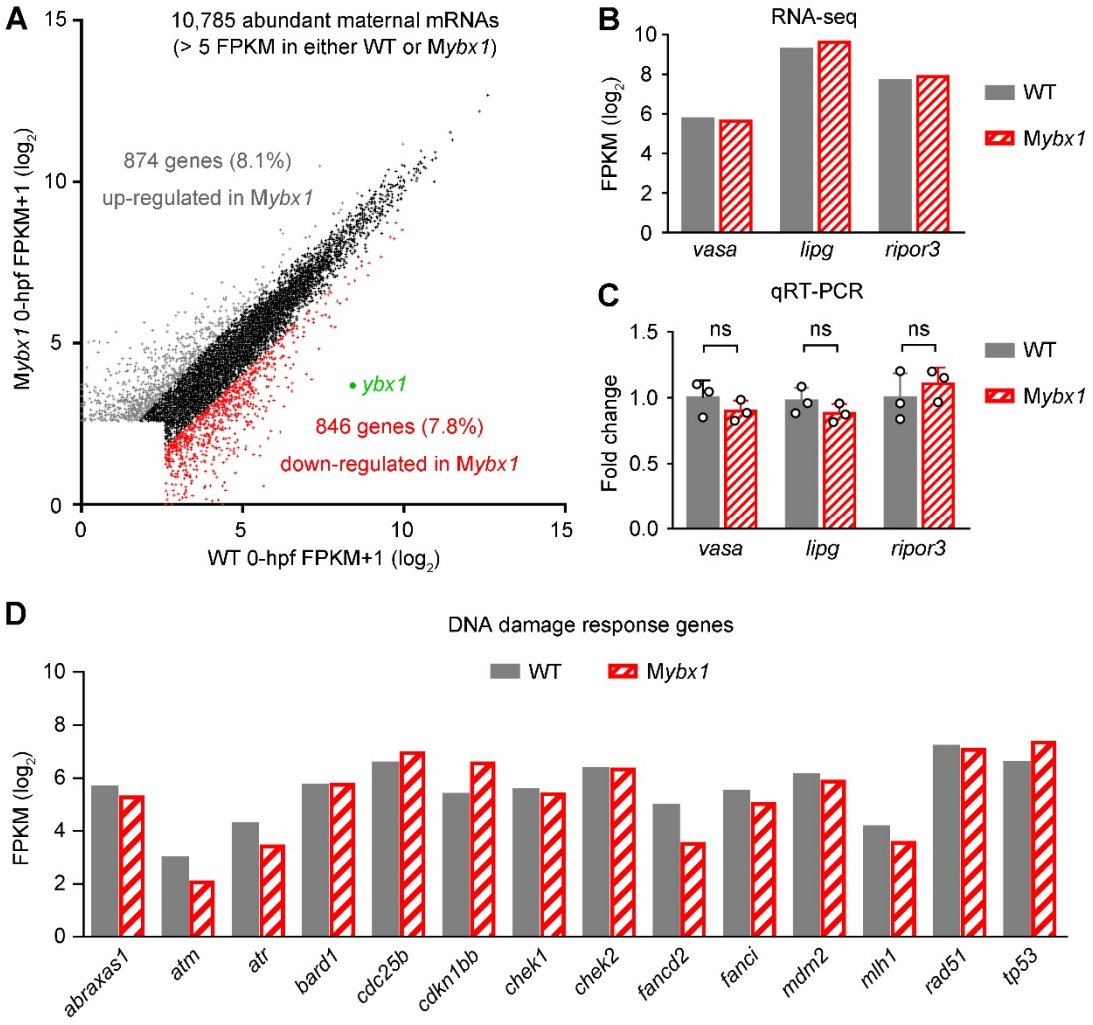

Fig. S4. Maternal transcriptome analysis of WT and M*ybx1* embryos. (A) Plotting of individual gene expression levels (FPKM+1, $\log_2$) in 0-hpf WT and M*ybx1* embryos. 10,785 genes with abundant maternal mRNA deposition (>5 FPKM in either WT or M*ybx1* embryo at 0 hpf) were plotted. Genes with >2-fold FPKM increases and >50% decreases in M*ybx1* were considered up and down-regulated genes, respectively. (B,C) Approximately equal expression levels of *vasa*, *lipg* and *ripor3* in WT and M*ybx1* embryos determined by RNA-seq and qRT-PCR data. *GFP* mRNA was injected at one-cell stage embryos and was used as the reference for qPCR. ns, not significant; n=3; Student's *t*-test. (D) Expression levels of DNA damage response genes in 0-hpf WT and M*ybx1* embryos.

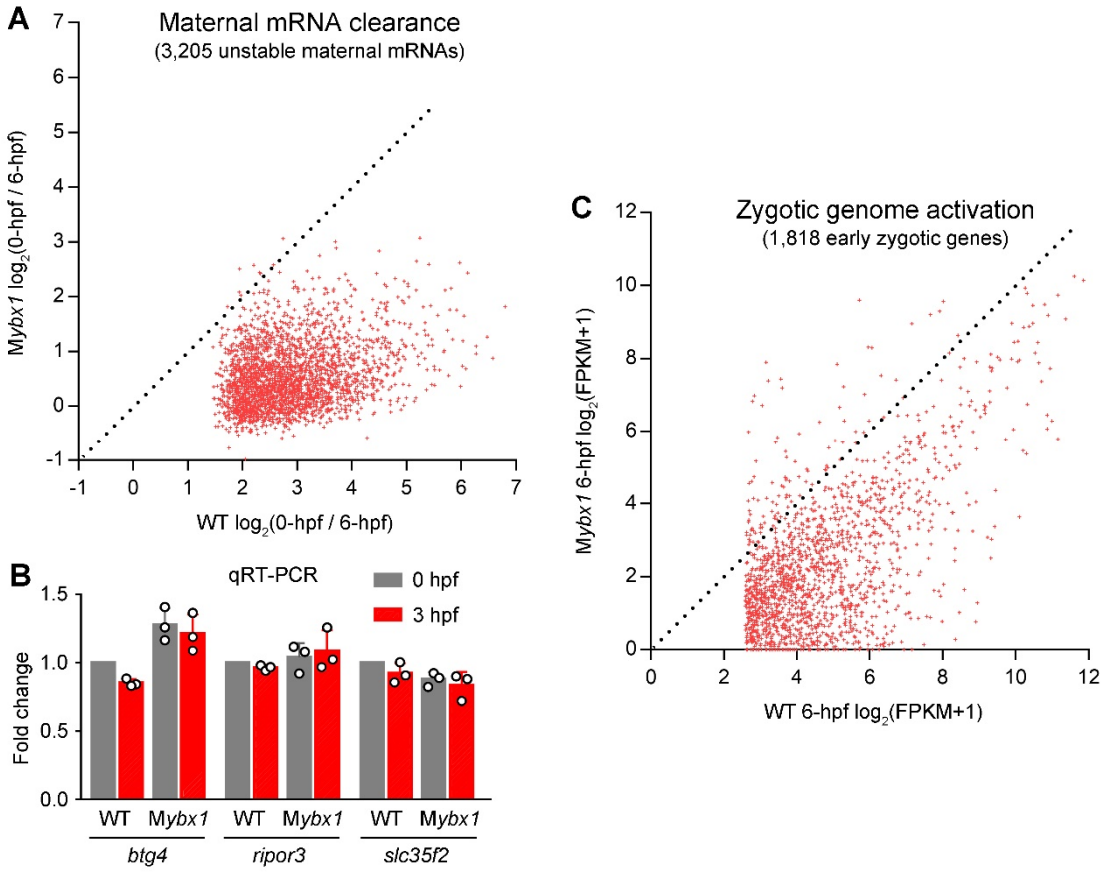

Fig. S5. Transcriptome analysis of the MZT process in M*ybx1* mutants. (A) Plotting of individual maternal mRNA degradation levels (0-hpf/6-hpf, log_2-scale) in WT and M*ybx1* embryos. 3,205 unstable maternal mRNAs were plotted. (B) qRT-PCR analysis of *btg4*, *ripor3* and *slc35f2* mRNA levels in 0-hpf and 3-hpf embryos. (C) Plotting of individual zygotic gene expression levels (log_2-scale) in 6-hpf WT and M*ybx1* embryos. 1,818 early zygotic genes were plotted. Dotted lines: y=x. (FPKM+1) values were calculated to include genes with 0 FPKM.

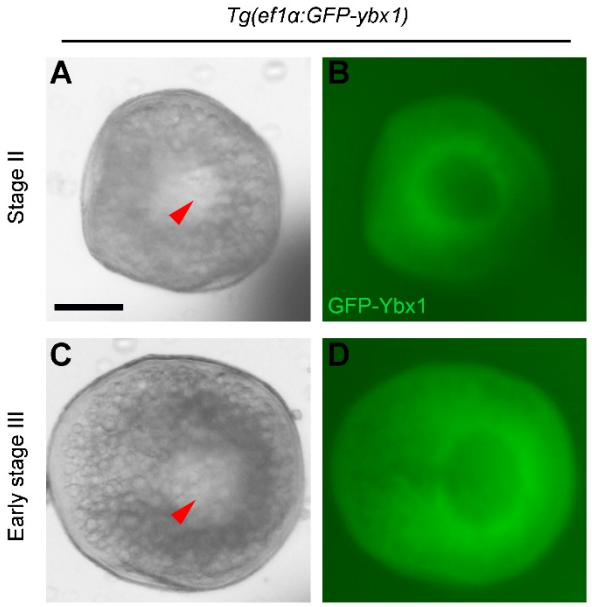

Fig. S6. GFP-Ybx1 expression in oocytes. Expression of GFP-Ybx1 fusion protein in *Tg(ef1α:GFP-ybx1)* oocytes at stage II (A,B) and early stage III (C,D). (A,B) Bright-field images. (C,D) Fluorescent images. Red arrowheads indicate oocyte nuclei. Scale bar: 100 µm.

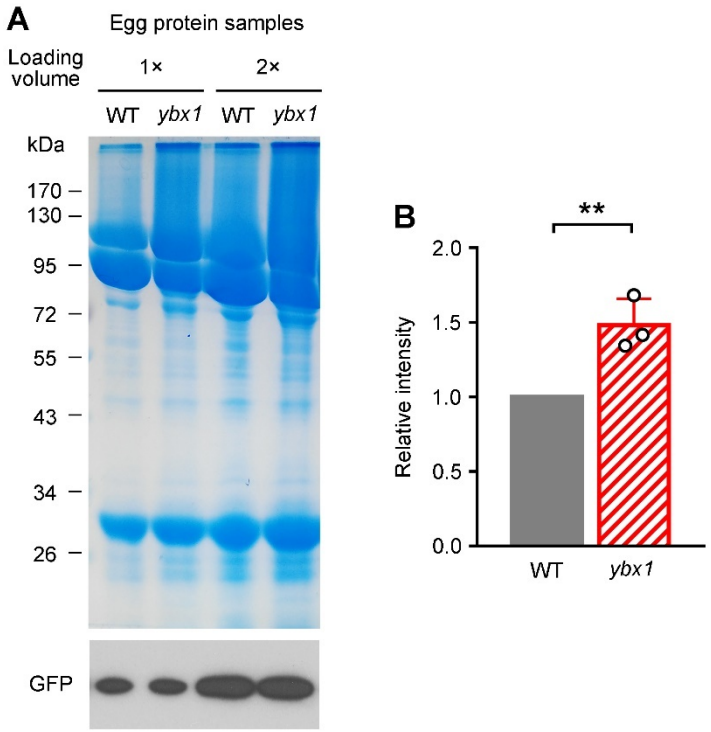

Fig. S7. Increase of global protein level in *ybx1* mutant eggs. (A) SDS-PAGE and Coomassie staining showing global protein levels in WT and *ybx1* mutant eggs. GFP protein was injected into eggs as the loading control. (B) Relative lane intensities quantified in the Coomassie staining images. Western blotting signal of GFP served as the control. ***P*<0.01; n=3; Student's *t*-test.

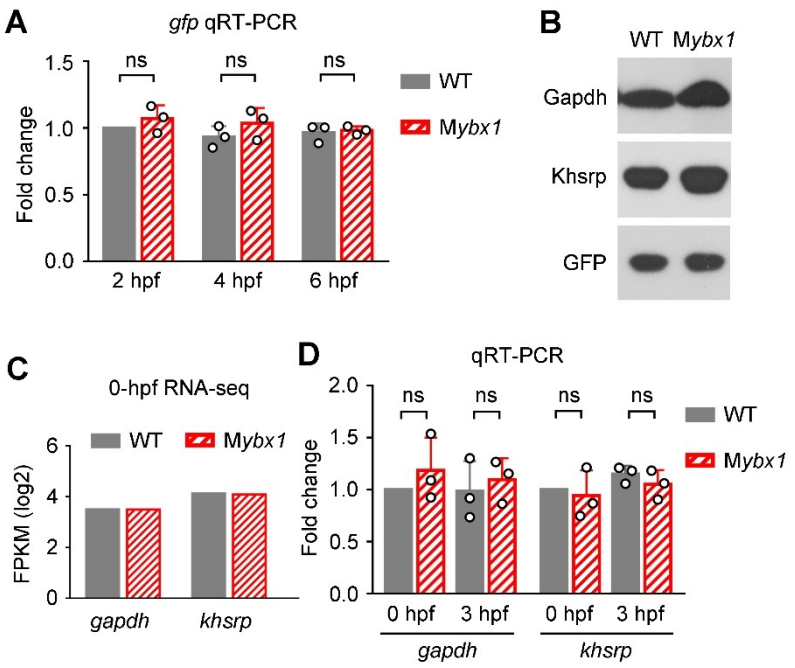

Fig. S8. Analysis of mRNA stability in WT and M*ybx1* embryos. (A) qRT-PCR analysis of injected *gfp* mRNA levels in 2-hpf, 4-hpf and 6-hpf embryos. (B) Western blotting analysis of Gapdh and Khsrp protein levels in 3-hpf WT and M*ybx1* embryos. Injected GFP protein was used as the loading control. (C) Gene expression levels of *gapdh* and *khsrp* in 0-hpf RNA-seq data. (D) qRT-PCR analysis of *gapdh* and *khsrp* mRNA levels in 0-hpf and 3-hpf embryos. ns, not significant; n=3; Student's *t*-test.

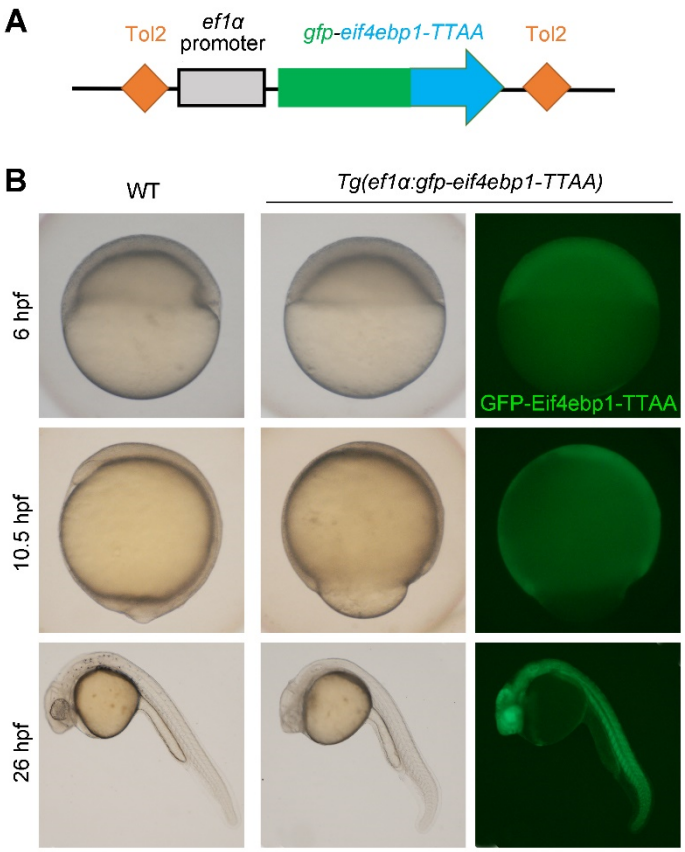

Fig. S9. The transgenic zebrafish line expressing a CA form of Eif4ebp1. (A) A diagram of the zebrafish *ef1α* promoter-driven *gfp-eif4ebp1-TTAA* transgene. (B) Bright-field and fluorescent images of *Tg(ef1α:gfp-eif4ebp1-TTAA)* embryos at 6 hpf, 10.5 hpf and 26 hpf, showing expression of Eif4ebp1-TTAA and the resulted developmental delay.

Supplementary tables

Table S1. PCR primers for *ybx1* mutant genotyping.

Primer	Sequence
ybx1-target-F	CTCAGTCCGTCCAGTTCGAT
ybx1-target-R	AAAATACCAGGCAGGACGCC
ybx1-wt-F	CAGCTACCGCGGGGGATAA
ybx1-mut-F	CGCAGCTACCGCGGTCATC

Table S2. qRT-PCR and RT-PCR primers.

Primer	Sequence
ybx1-F	TTCGACGTGGTAGAAGGGGA
ybx1-R	ACCTTCACCACCCTCTGTCA
vasa-F	CCAGAGTCTGACACTCCATTAGCTC
vasa-R	GAGCACTGAAGGCAACTTCCTC
gfp-F	GTGGTGCCCATCCTGGTC
gfp-R	CCGGTGGTGCAGATGAACTT
btg4-F	TGTCATGCCGGTATGGTGAA
btg4-R	GTTGGGATGCATTTGGGCTC
casd1-F	GCATTCTGGAATCTGGCCCT
casd1-R	TGACCACAGCAAATCGGTCC
cldnd-F	ACAATGGCATCTGTTGGGCT
cldnd-R	GTTCATCCAGAGGCCTTCCC
lipg-F	CACTTGGGGTCCTCGTTCTT
lipg-R	GTAGTGCAATCGTTTCCTGGG
ripor3-F	TGAGGAAGGGACTCAAGGACT
ripor3-R	ACAGCCGCCACTGAATACAA
slc35f2-F	TGGGGTGCAAATGGCTATACT

slc35f2-R	TTACCACCACAGGCACGAAA
acadl-F	CCACATCAGCAGCATGTTCG
acadl-R	CGTTTTGCCTGAACAGGTCG
cd82b-F	CAGCTGCTCCACGGATCTTC
cd82b-R	ATGCAACCCAGGAATCCCAT
apoeb-F	CACACAAACTGACGGCATGG
apoeb-R	GCATATGGGGTCATCTGGG
cxcr4b-F	GCGCCTTTTTGAGCACACTT
cxcr4b-R	ATTGCTGACTGAGAGGTCGC
dusp6-F	TTGCAGGCATCAGTCGTTCT
dusp6-R	TCCTAACGTGCGCTCAAAGT
fgfr4-F	CAGAGCGACGTATGGTCTTT
fgfr4-R	AGGTGTCCTCACAAGATGGA
grhl3-F	ATGGAGAGGACGGCAAACAG
grhl3-R	AGGTGTGGCCTCCAGAAAG
nnr-F	CGCAGAGATGGACAGCGATT
nnr-R	ATATTGGCCTCGTCTGGAGC
vent-F	AAACTCAGGTGAAGACGTGG
vent-R	AGAAGTAGCAGCGTGTGAAC
wnt11-F	CACACAGAACGCCAAACAGG
wnt11-R	CAGACGTATCTCTCGACGG
gapdh-F	ACAGCAACACAGAAGACCGT
gapdh-R	GGCAGGTTTCTCAAGACGGA
khsrp-F	AGAGTGTTCGTCCTTCGTCG
khsrp-R	CCACTGTCTGGAGCGATCTG
xbp1-slicing-F	AGGAGATCAGACTCAGAGTCTG
xbp1-splicing-R	GAGACAAGACGAGTGATCTGCT
actb2-F	ATGGATGATGAAATTGCCGCAC

actb2-R	ACCATCACCAGAGTCCATCACG
atf3-F	ATCACAAACACACGCGCCTA
atf3-R	TTTGTGAAGTCGTCCAGCGT

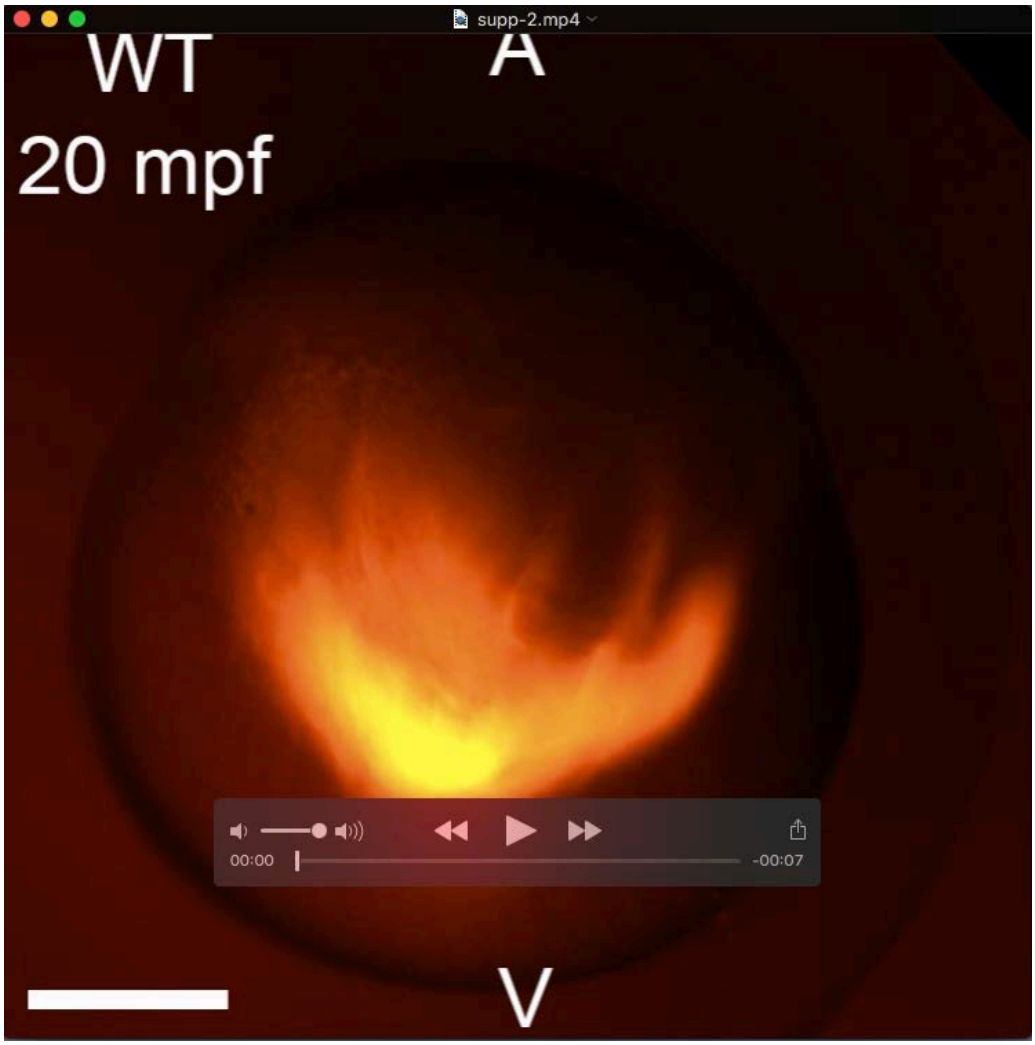

Movie 1. Cytoplasmic movement in a WT embryo from 20 mpf to 40 mpf. Rhodamine dye was injected at 10 mpf and embryos were imaged from 20 mpf to 40 mpf. The persistent cytoplasmic streaming that transports rhodamine to the animal pole can be visualized. 8 embryos were observed and this movie shows the representative result. A, animal pole; V, vegetal pole. Scale bar: 200 μm.

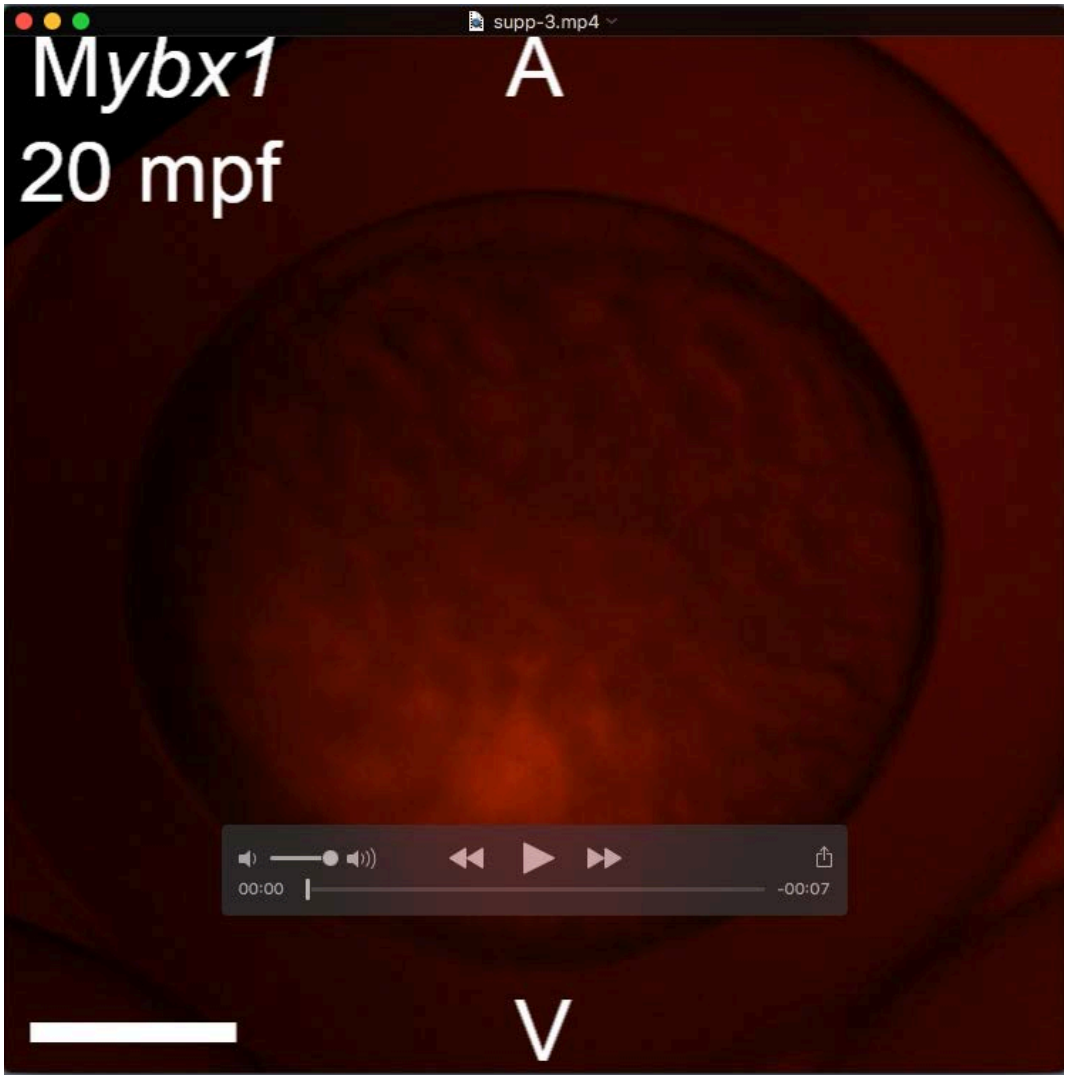

Movie 2. Cytoplasmic movement in an M*ybx1* embryo from 20 mpf to 40 mpf. Rhodamine dye was injected at 10 mpf and embryos were imaged from 20 mpf to 40 mpf. Due to the opaqueness of M*ybx1* embryos, the rhodamine fluorescence is relatively weak and scattered. The cytoplasmic movement is stagnant and the transportation of rhodamine is highly inefficient. 5 embryos were observed and this movie shows the representative result. A, animal pole; V, vegetal pole. Scale bar: 200 μm.

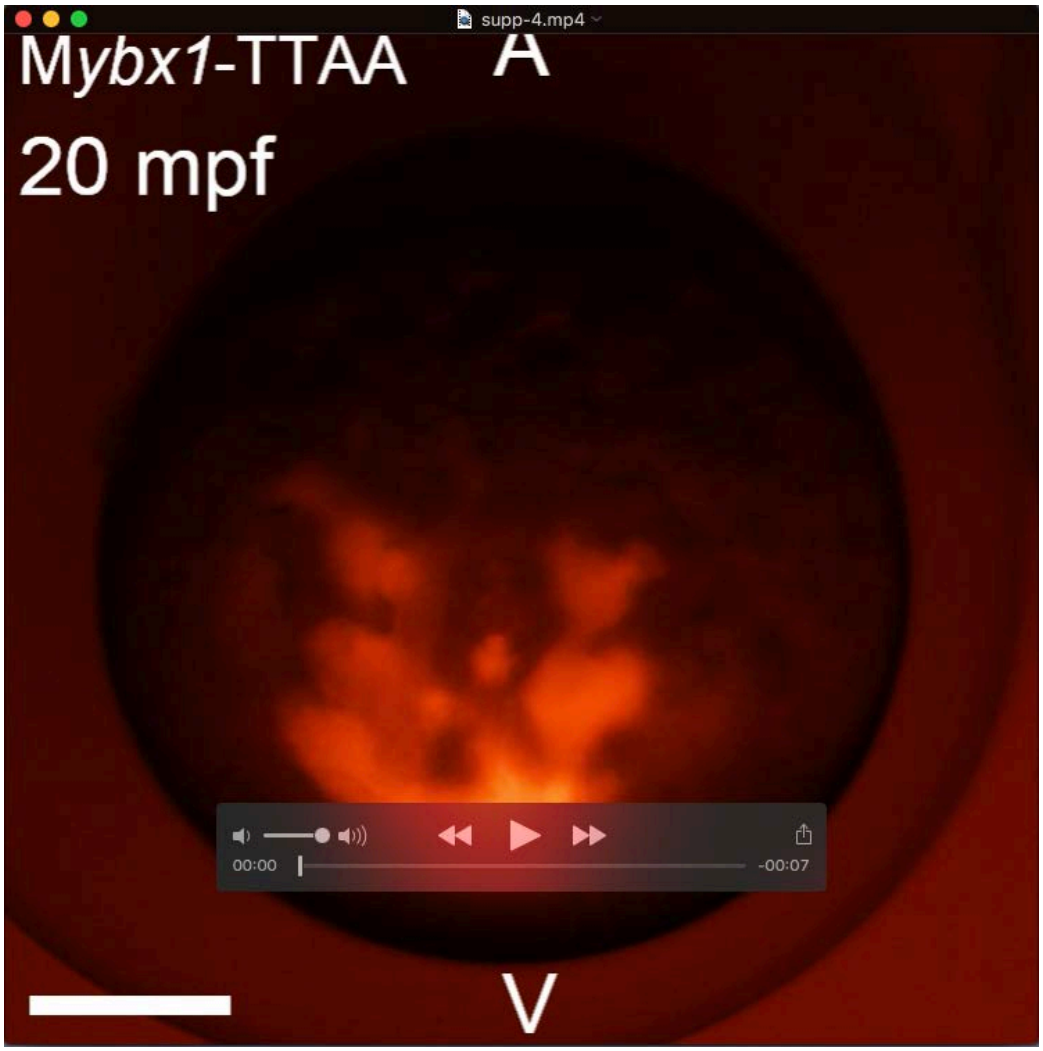

Movie 3. Cytoplasmic movement in an M*ybx1*-TTAA embryo from 20 mpf to 40 mpf. Rhodamine dye was injected at 10 mpf and embryos were imaged from 20 mpf to 40 mpf. Compared to M*ybx1* embryos (Movie 2), the cytoplasmic movement is partially restored. 6 embryos were observed and this movie shows the representative result. A, animal pole; V, vegetal pole. Scale bar: 200 μm.